Supplement to manuscript:

Impact of NO_x on secondary organic aerosol (SOA) formation from α-pinene and β-pinene photo-oxidation: the role of highly oxygenated organic nitrates

By: I. Pullinen, S. H. Schmitt, S. Kang, M. Sarrafzadeh, P. Schlag, S. Andres, E. Kleist, T. F. Mentel, F. Rohrer, M. Springer, R. Tillmann, J. Wildt, C. Wu, D. Zhao, A. Wahner and A. Kiendler-Scharr

In the supplement we will derive lower and upper limits for the calibration coefficient of the NO_3^--CIMS for HOM (Section S1) and describe how we determined and separated HOM organic nitrates in the high resolution mass spectra (Section S2). In Section S3 we show details of the normalization of HOM concentrations to particle surface and chemical turnover (Experiment 2 in Table 1 of main the manuscript). Gas-phase yields of organic nitrates (ON) for a β-pinene photo-oxidation experiment are described in Section 4 as well as the derivation of $OrgNO_3$, the mass of nitrate bound to organic moieties. In Section S5 we will discuss pattern of HOM-ON as function of NO_X in relation to their mass median HOM. Section S6 provides the peak lists obtained from high resolution spectra from α-pinene and β-pinene in presence of NO_X.

We will refer to several reactions and figures given in the main manuscript using the according numbering.

S1 Estimation of lower and upper limit of the calibration coefficient for HOM

S 1.1 Relative transmission curve of the $NO_3^- - CIMS$

The relative transmission curve was determined with perfluoropentanoic acid C_4F_9COOH. C_4F_9COOH forms several clusters with nitrate ions. In addition it can be deprotonated or fragmented resulting in $C_4F_9^-$. The molecular masses of the observed ions are listed in Table S1 and cover a range of about 700 Th.

Adding C_4F_9COOH in varying amounts to the analyte stream (6.4-57 ppb) led to depletion of the reagent ion and reagent ion clusters and to formation analyte (cluster) ions in varying ratios. The total ion signal was not much affected by the presence of C_4F_9COOH, it was decreasing by about 10% at the highest load of C_4F_9COOH, thus the highest load of higher mass dimers (Figure S1, black). Under the assumption that the total concentration of ions remains constant, we optimized the mass dependent transmission relative to the NO_3^- signal (m/z = 62 Th) over the range 62 – 791 Th. The resulting transmission function was flat and

monotonously decreasing with increasing molecular weight of the ions, reaching eventually 86% at 791 Th (Figure S1, blue).

Table S1 Ions for relative transmission

Ions	m/z [Th]
$HNO_3 \cdot NO_3^-$	124.984
$(HNO_3)_2 \cdot NO_3^-$	186.971
$C_4F_9^-$	218.986
$C_4F_9COO^-$	262.975
$C_4F_9COOH \cdot NO_3^-$	325.971
$C_4F_9COOH \cdot HNO_3 \cdot NO_3^-$	388.967
$C_4F_9COOH \cdot (HNO_3)_2 \cdot NO_3^-$	451.962
$C_4F_9COOH \cdot (HNO_3)_3 \cdot NO_3^-$	514.958
$C_4F_9COOH \cdot C_4F_9COO^-$	526.959
$(C_4F_9COOH)_2 \cdot NO_3^-$	589.954
$(C_4F_9COOH)_2 \cdot C_4F_9COO^-$	790.942

This is different to the observations by Heinritzi et al. (2016), but in agreement with the flat transmission function determined by Ehn et al. (2011), for another API-TOF of the same type, without CI source, though.

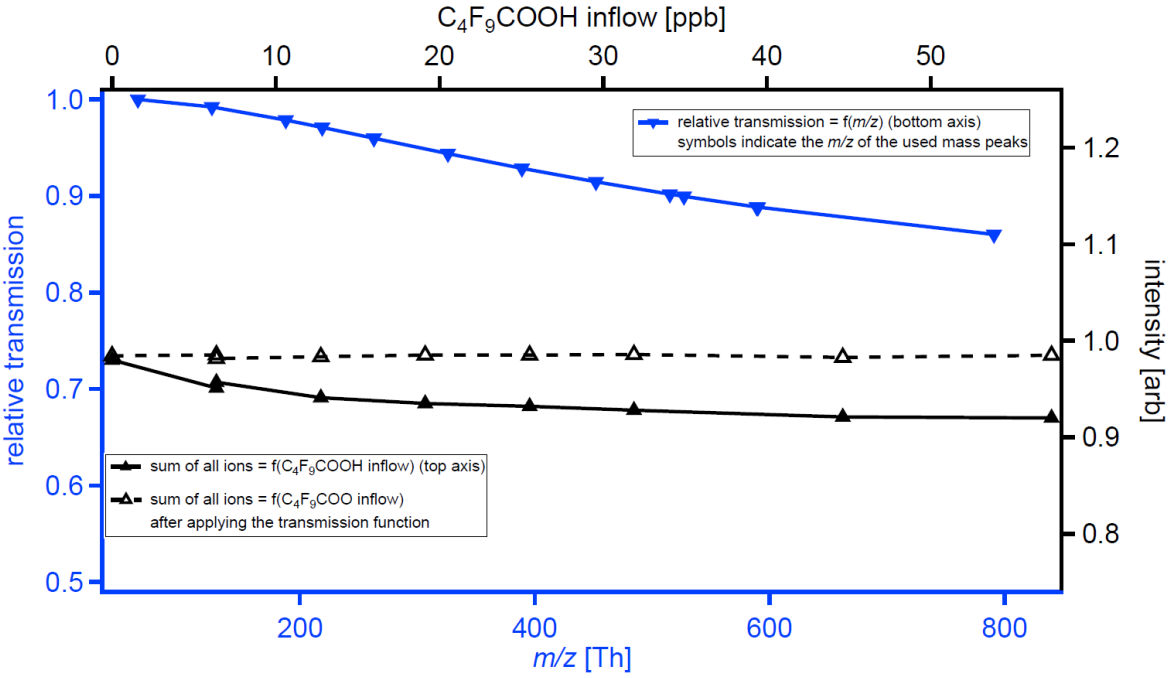

Figure S1: Relative transmission function for the NO_3^--TOF-CIMS. The blue parts show the relative transmission as a function of mass to charge ratio (*m/z*). The black parts shows the drop of the sum of all ions with increasing load of C_4F_9COOH, which changed ratio of reagent ions / analyte ions and the distribution of analyte (clusters) ions with different *m/z* (continuous line). The dashed line shows the sum of all ions after applying the transmission correction, which was used for optimization.

S 1.2 Calibrations of the NO_3^--CIMS with H_2SO_4.

To calibrate the NO_3^--CIMS with sulfuric acid we generated H_2SO_4 in situ in JPAC by SO_2 oxidation. SO_2 was taken from a gas cylinder (0.94 ppm SO_2 in N_2) and added at flows of 31.9 and 16.5 mL min^{-1} to the chamber air which led to mixing ratios at chamber inlet of 0.97 ppb and of 0.5 ppb, respectively. After the last measurement the addition of SO_2 was stopped at otherwise unchanged conditions and we measured the temporal behaviour of the MS signals, while the SO_2 was flushed out to zero in order to determine background and possible interferences. The ion signals from the NO_3^--CIMS were normalized to the sum of all ions in order to minimize effects by the performance of the mass spectrometer. In the following we will term such normalized data as normalized counts (nc).

We added (*E*)-2-butene in a mixing ratio of 18.2 ppb as tracer for OH at chamber inlet. (*E*)-2-butene was chosen because it did not produce detectable amounts of particles upon photo-oxidation. OH production was induced by ozone photolysis in presence of water vapour as usual. The OH concentrations in steady state were determined to $(3.3 \pm 0.8)\times10^7$ cm^{-3} from the observed (*E*)-2-butene consumption by applying $k_{OH+(E)\text{-}2\text{-}butene} = 6.4\times10^{-11}$ cm^3 s^{-1}, $k_{O3+(E)\text{-}2\text{-}butene} = 1.0\times10^{-16}$ cm^3 s^{-1} (Atkinson, 1997), and the observed $[O_3]_{SS}$. The [OH] remained about the same when SO_2 concentrations were changed. This is related to the low reactivity of SO_2 compared to that of (*E*)-2-butene.

In the resulting mass spectra we observed several peaks with intensities significantly above the detection limit. Dominant peaks were those of the reagent ion NO_3^- and its oligomers which covered more than 95 % of the signal intensities. Strong peaks arising from H_2SO_4 were found at *m/z* = 97 Th ($H^{32}SO_4^-$ ion), *m/z* = 160 Th ($H^{32}SO_4 \cdot HNO_3^-$) and *m/z* = 223 Th ($H^{32}SO_4 \cdot (HNO_3)_2^-$). To obtain the H_2SO_4 concentration we summed up the signal intensities of the three peaks and multiplied the sum by 1.04 in order to consider the ^{34}S isotopes. From the measurements after the SO_2 inflow was stopped we ensured that the selected peaks were related only to H_2SO_4 and not interfered by (*E*)-2-butene oxidation products.

The reaction of OH with SO_2 is the rate limiting step of the H_2SO_4 production as the reaction of HSO_3 with H_2O is much faster at the mixing ratio of water vapour of 1.06 % than the oxidation of SO_2 by OH:

$$P(H_2SO_4) = k_{SO2} \cdot [SO_2] \cdot [OH] \quad \text{(S1)}$$

In Eq. S1, k_{SO2} is the rate constant (1.1×10^{-12} cm^3 s^{-1}, Atkinson et al., 2004) and $[SO_2]$ is the SO_2 concentration in our chamber. As OH reacts with SO_2 the $[SO_2]$ is depleted in the chamber according to Eq. S2:

$$\frac{d[SO_2]}{dt} = \frac{F}{V} \cdot ([SO_2]_0 - [SO_2]) - k_{SO2} \cdot [SO_2] \cdot [OH] \quad \text{(S2)}$$

In Eq. S2, V is the volume of the chamber, F the air flow through the chamber, $[SO_2]_0$ represents the SO_2 concentration at chamber inlet and $[SO_2]$ represents the SO_2 concentration in the chamber.

Setting the differential equation (S2) to steady state and solving for $[SO_2]_0$ / $[SO_2]$ leads to:

$$\frac{[SO_2]_0}{[SO_2]} = \frac{V}{F} \cdot k_{SO2} \cdot [OH] + 1 \quad \text{(S3)}$$

The concentration of SO_2 in the chamber was calculated from $[SO_2]_0$ and [OH] and we obtained mixing ratios of 0.87 and 0.45 ppb, respectively. Using these mixing ratios, the production rates of H_2SO_4 were determined to $P(H_2SO_4) = 8.03\times10^5$ cm^{-3} s^{-1} and 4.15×10^5 cm^{-3} s^{-1} in the two experiments.

Particle formation was not observed and the only important loss of H_2SO_4 was its deposition at the surfaces of the chamber. Wall losses of H_2SO_4 had been determined in a similar experiment, but OH production was switched off and H_2SO_4 production was stopped. We observed an exponential decay of H_2SO_4 with a lifetime 87±5 s (loss rate $L_W = 1/\tau = 0.012\pm0.001$ s^{-1}).

Knowing the production rate of H_2SO_4 and its first order loss rate allowed for calculating it's concentrations in the chamber:

$$[H_2SO_4] = \frac{P(H_2SO_4)}{L(H_2SO_4)} \quad \text{(S4)}$$

Figure S2 shows the signal intensities of the sulfuric acid related peaks as a function of $[H_2SO_4]$ which was determined according to Eq. S4.

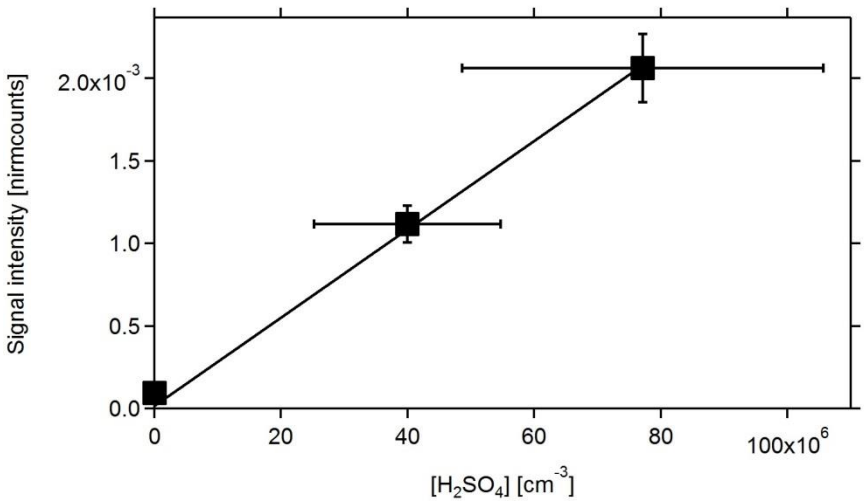

Figure S2: Plot of normalized and summed signal intensities versus [H_2SO_4] concentration. The solid line shows the linear regression forced through zero. The inverse of the slope was used to determine calibration factor C_{H2SO4}. The main uncertainty in the determination is due to the uncertainty of [H_2SO_4] that was estimated to ± 37 %.

The signal intensity at *m/z* 97, 160, and 223 Th measured after the flush out of SO_2 from the chamber was similar to that observed in many other experiments. It was therefore assumed to represent the background level of H_2SO_4 in our chamber when the UV light is on (~2×10^6 cm^{-3}). Since this signal is real, we forced the regression through zero. The inverse of the slope of the regression line gave us the calibration coefficient C_{H2SO4} in units of molecules cm^{-3} nc^{-1}. C_{H2SO4} was determined to $(3.7 \pm 1.2)\times10^{10}$ molecules cm^{-3} nc^{-1}. The relative uncertainty of C_{H2SO4} was estimated to ± 37 % from the uncertainty of [OH] (~ 20 %), the uncertainty of the SO_2 concentration (~5 %), and the uncertainty of L_W (~ 25%) using error propagation.

C_{H2SO4} as determined here is about an order of magnitude higher than that determined by Ehn et al., (2014) who found 4 - 5×10^9 molecules cm^{-3} nc^{-1}. This discrepancy might be due to a lower performance of the NO_3^--TOF-CIMS during our measurements, and we used C_{H2SO4} = 3.7×10^{10} molecules cm^{-3} nc^{-1} for further calculations. As described by Ehn et al. (2014) and Hyttinen et al. (2017), HOM with 6 and more O-atoms are detected with similar sensitivity as H_2SO_4. We therefore also used C_{H2SO4} to calculate HOM concentrations by setting C_{HOM} = C_{H2SO4}.

S1.3 Comparison of HOM condensation and SOA formation

The high sensitivity of the NO_3^--CIMS to sulfuric acid is due to the effective deprotonation of H_2SO_4 and formation of clusters with the nitrate reagent ions, that is essentially collision limited. The cluster formation of HOM nitrate clusters is supposedly also collision limited (Ehn et al., 2014; Kirkby et al., 2016; Hyttinen et al., 2017). Setting $C_{HOM} = C_{H2SO4}$ allows for calculation of concentrations or mixing ratio of HOM, at least their lower limit, since the sensitivity for the detection of HOM can only be lower than the collision limit. An upper limit for C_{HOM} can be derived by applying the effective uptake coefficients of HOM derived in the main manuscript, which give the maximum potential of HOM to form particulate matter. In the main manuscript, we showed that HOM with more than 6 O-atoms efficiently contribute to particle formation with uptake coefficients close to one. The mass of those HOM expected to condense, can be calculated by summing up the mass weighted gas-phase concentrations in absence of particles. Since other compounds can also contribute to SOA, an upper limit for C_{HOM} can be determined from the measured increase of particle mass.

We applied $C_{HOM} = C_{H2SO4}$, determined HOM concentrations and summed up the concentrations of all HOM with masses between 230 and 550 Da as they all are expected to contribute to particle formation.

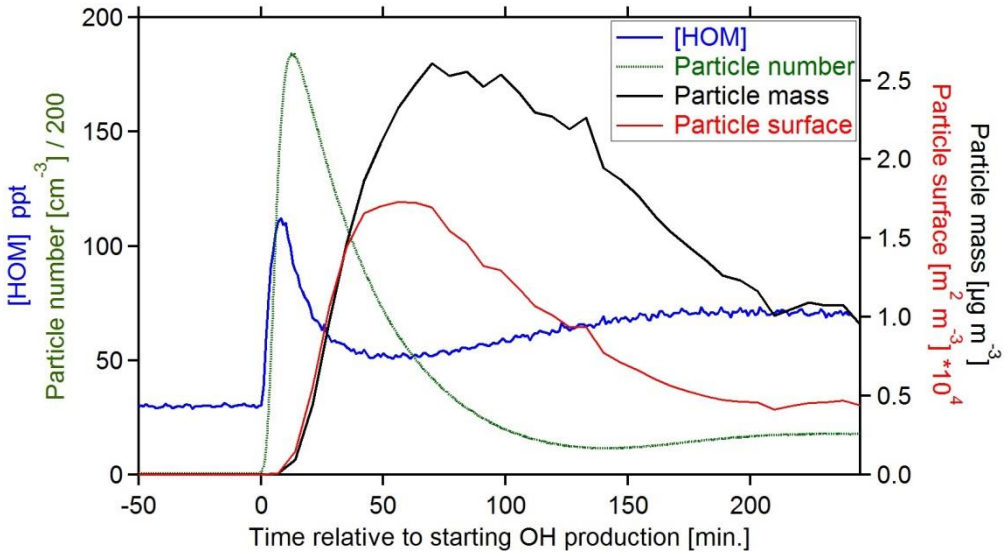

Figure S3: Temporal evolution of the mixing ratios of the HOM sum (molecular weights between 230 and 550 Da, blue line), particle number (green dashed line, divided by 200), particle surface (red line, multiplied by 10^4), and particle mass (black line). Data from α-pinene experiment with $[\alpha\text{-pinene}]_{SS}$ = 1.4 ppb and $[NO_X]_{SS}$ = 0.3 ppb. HOM from ozonolysis α-pinene were observable before OH production was induced at t = 0 min.

A typical experiment with α-pinene was performed as follows. About 10 ppb α-pinene were added to the chamber while [OH] was about 4×10^7 cm^{-3}. Without addition of NO_X, we found HOM mixing ratios of up to 120 ppt, short after the OH production was started (Figure S3). When new particle formation (NPF) set on, the HOM mixing ratio decreased with increasing particle formation. The HOM mixing ratio went through a minimum that appeared aligned to the maximum particle surface and increased again as soon as particle surface decreased. After 200 min. we approached steady state for particle number, particle surface, particle mass, and gas-phase HOM.

We can explain the relation of HOM mixing ratio, particle surface, and particle mass observed in Figure S3. After starting the OH production it took several minutes to reach maximum HOM mixing ratios. The amount of HOM condensing on the particles increased with increasing particle surface until the particle surface decreased again. Decrease of particle surface is due to coagulation and flush-out of particles. This reduced HOM condensation on the particle and caused decreasing particle mass. About 3 hours after starting the OH production, a situation close to steady state is reached with only small fluctuations, where particle production, HOM production and condensation, as well as flush-out balance.

We calculated the mass transferred by HOM condensation from the gas phase to the particle phase by applying the mass balance equation Eq. S5:

$$\frac{dP_M}{dt} = -\frac{F}{V} \cdot [P_M] + [HOM]_{LP} \cdot L_P \qquad \text{(S5)}$$

Herein, $[P_M]$ is the particle mass concentration in the reaction chamber and $[HOM]_{LP}$ represents the fraction of HOM that condense on particles and not are lost on the chamber walls. L_P is the loss coefficient for condensation of HOM on particles. At steady state conditions and in consideration of $\frac{F}{V} = \frac{1}{\tau}$ with τ = residence time of the air in the chamber, it follows:

$$[P_M] = [HOM]_{LP} \cdot L_P \cdot \tau \qquad \text{(S6)}$$

L_P was determined and its dependence on particle surface is in accordance with kinetic gas theory (see main text, Section 2.4, Eq. 7). To determine $[HOM]_{LP}$ we used the methods described in Sarrafzadeh et al. (2016). Therein the fraction of HOM condensing on particles and not lost on the chamber walls is given by:

$$F_P(HOM) = \frac{L_P(HOM)}{L_P(HOM) + L_w(HOM)} \quad \text{(S7)}$$

Thus, Eq. S6 can be reformulated using Eq. S7 to:

$$[P_M] = [HOM] \cdot \frac{L_P^2(HOM)}{L_P(HOM) + L_w(HOM)} \cdot \tau \quad \text{(S8)}$$

Eq. S8 is only valid for steady state conditions where [HOM] is constant. As can be seen from Figure S3, [HOM] still varied somewhat due to the variable particle surface even under overall near steady state conditions. We therefore replaced the [HOM]×τ by the running value $\Sigma^{t}_{t-\tau}$[HOM], i.e. the sum of HOM mixing ratios measured over one residence period τ of about 46 min. before the respective measurement of the particle mass. This way the $[P_M]$ originating from HOM condensation was predicted (under application of $C_{HOM} = C_{H2SO4}$). Figure S4 compares exemplarily the observed particle mass concentration with the predicted mass from HOM condensation beginning with the onset of achieving steady state conditions.

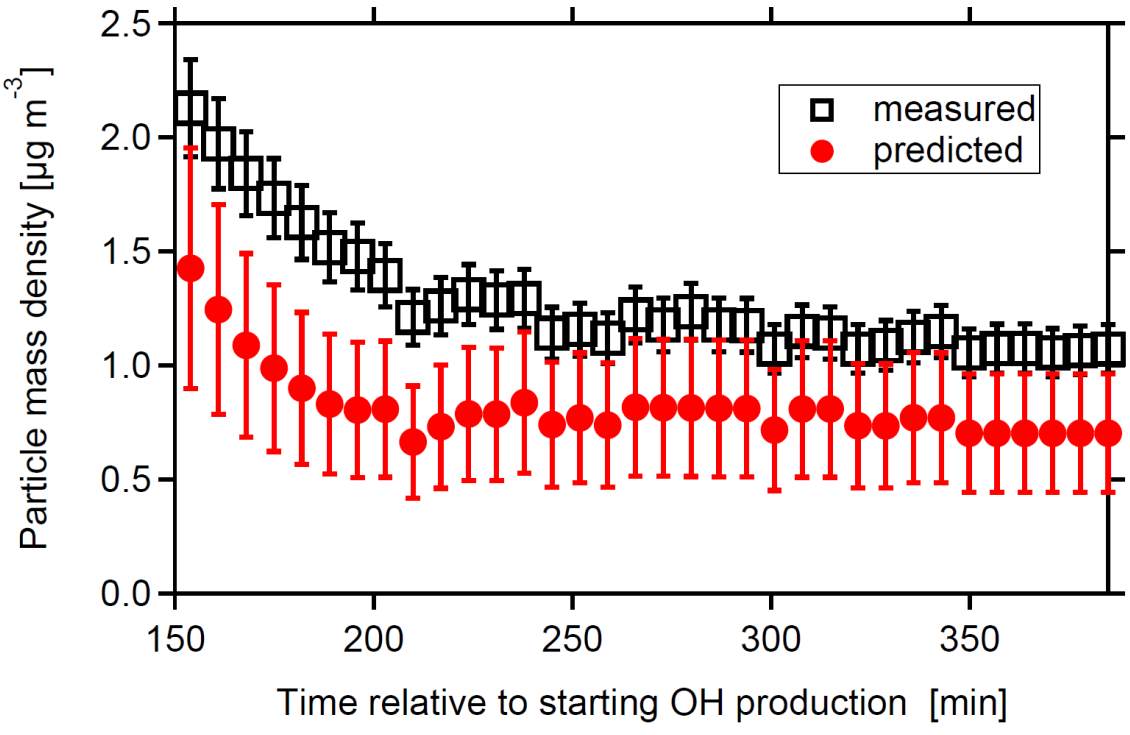

Figure S4: Particle mass from SMPS measurements (black squares, error ±10%) and particle mass predicted by HOM condensation (red circles, error ±37%). The particle mass derived from SMPS was calculated from the measured particle number concentration with a density of 1.2 g/cm^3. Experiment with α-pinene ($[\alpha\text{-pinene}]_0$ ~ 11 ppb, $[\alpha\text{-pinene}]_{SS}$ ~ 1.4 ppb, $[NO_X]_{SS}$ ~ 0.3 ppb).

At steady state conditions for t > 250 min, particle mass predicted from HOM condensation parallels the observed particle mass (Figure S4). Figure S4 indicates that indeed a large fraction of the measured particle mass was produced by the mass of condensing HOM. Six more experiments of the same type as shown in Figure S3 showed that on average (57± 13)% of the particle mass can be explained by condensation of HOM. As HOM condensation cannot form more particle mass than measured and assuming all SOA stemmed from HOM led to an upper limit for C_{HOM} ~ 6.5×10^{10} molecules cm^{-3} nc^{-1}. As the upper and lower limit of C_{HOM} differed by less than a factor of 2, we concluded that we can constrain HOM concentrations within a factor of 2. Note, for HOM concentrations given in the main text, we used 3.7×10^{10} molecules cm^{-3} nc^{-1} as calibration factor and HOM concentrations might have been maximum a factor of 2 higher.

At the conditions in our chamber where monoterpene mixing ratios were typically below 10 ppb, on average *at least* 57 % of the particle mass was produced by condensation of HOM. From this we can confirm that SOA play a crucial role in particle mass formation.

From these findings we furthermore concluded, that the difference we found between the fraction of organic bound nitrate ($OrgNO_3$) in particles (main text Figure 7) and in the HOM contributing to particle mass (main text Figure 8) cannot be explained by a higher sensitivity of the NO_3^--CIMS for HOM-ON than for other HOM-termination products. The upper limit of C_{HOM} indicates that at least every second collision of a non-organic nitrate HOM with NO_3^- leads to its detection as a cluster. Hence the maximum sensitivity for a HOM-ON can be at maximum two times higher than that for other termination products. However, with a factor of 3 to 4 the difference between $OrgNO_3$ found in HOM and in particles was nearly twice as high. An explanation of this large difference solely by different sensitivities seems unrealistic.

S2. Identification of organic nitrates in high resolution mass spectra

High resolution data were analysed using Tofware (v.2.5.11, Tofwerk AG and Aerodyne Research, Inc.) and Igor Pro (7.08) (Wavemetrics). Data was averaged over 1 minute with a built in pre-averaging unit function. Instrument functions (peak shape, peak width and baseline) were acquired from the built in function that uses the algorithm described in Stark et al. (2015). The mass calibration, instrumental line shape and peak width were determined by following standard procedures. Mass calibration accuracy was better than 5 ppm. The mass resolution (m/Δm) for the m/z range 300-400 was about 5000.

The following procedure was used for peak identification. We fitted the observed shape of the peak under investigation applying instrument peak shape and peak width function determined above. When needed, we increased the number of fitted peaks until the residuals showed no big bias towards missing components. Once we determined how many peaks were under the measured peak, molecular formulas consisting of C, H, O, and N-atoms were assigned to the fitted peaks. Therein less than 15 ppm of error was allowed between the fit maximum and the exact formula mass.

In addition to the mass defect criterion, the following constraints were considered for peak identification. Only inherent meaningful molecular formulas were assigned and ^{13}C isotopy must be commensurate to the assignment. The time behaviour of the expected molecule according to the formula must be commensurable with expectation for the photochemical system chemical system, e.g. significant amounts of ON can only be formed in presence of sufficient NO_X. As an example for the identification of a HOM-ON, Figure S5 shows the peaks at m/z = 263 Da under different NO_X conditions, respectively. (Note, we expect HOM-ON with the functional group -O-NO_2 and with the functional group -OO-NO_2, i.e. PAN like compounds. They arise from HOM peroxy radicals or HOM acyl peroxy radicals with NO and NO_2, respectively, and cannot be distinguished in our reaction systems by MS alone.)

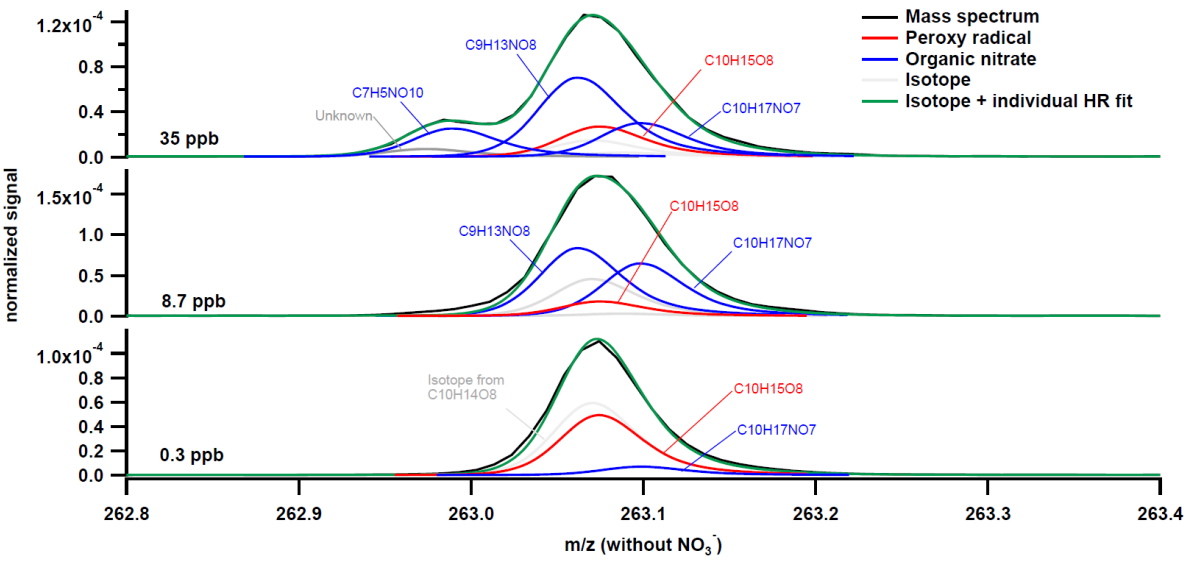

Figure S5: Separation of RO_2 (red) and organic nitrates (blue) in high resolution spectra at the integer mass of 263 Da. Steady state [NO_X] increase from 0.3 ppb in the lower to 35 ppb in the top panel. Mass spectra were normalized to the sum of all ion signals. With increasing [NO_X] the compound $C_7H_5NO_{10}$ appears which is probably formed heterogeneously at the chamber walls

S3. Normalization of HOM concentration to actual particle surface and actual [OH]

Essentially, we want to consider relative changes of HOM concentrations. We assumed overall the same sensitivity for all HOM with O > 6 in accordance with Riva et al. (2019) for nitrate CIMS. Under these conditions the normalization procedures described in the following are independent of an exact calibration. Adding to or removing NO_X from a photochemical system directly impacts OH concentrations by reactions R1 and R2. NO_X furthermore suppresses new particle formation (NPF, Wildt et al., 2014) which leads to reduction of the actual particle surface and thus the condensation sink for HOM with increasing [NO_X]. The actual OH concentration affects the turnover of the precursor, thus the production of $RO_2\cdot$ and HOM. In addition, loss of condensational sink impacts on condensational loss of HOM. Both factors change the observed HOM gas-phase mixing ratio and can superimpose the impacts of NO_X on the peroxy radical chemistry itself. In order to separate the chemical impacts of NO_X on HOM-peroxy radical chemistry we took out the effects of [OH] and the condensational sink as much as possible. This was achieved by normalizing the HOM mixing ratio to particle free conditions and to a certain reference turnover of the precursor molecule. To derive the HOM mixing ratio for a particle free chamber in cases where NPF could not be suppressed despite optimized boundary conditions, we applied a similar approach as to determine the effective uptake coefficients of HOM (Section 3.5) and the wall loss of HOM (Sarrafzadeh et al., 2016).

Both were based on the ratio of signal intensities (S) or here concentrations (c) of HOM in presence and absence of aerosols (Equation 1):

$$\frac{S(HOM)^0}{S(HOM)} = \frac{c(HOM)^0}{c(HOM)} = \frac{L_W(HOM)+L_P(HOM)}{L_W(HOM)} \quad \text{(S9)}$$

In Equation S9, $S(HOM)^0$ and $c(HOM)^0$ are the signal intensities and mixing ratio as determined for an individual HOM at negligibly low particle surface (< 10^{-5} m^2 m^{-3}). $S(HOM)$ and $c(HOM)$ are the signal intensities and the respective mixing ratio measured in the presence of significant particle surface under otherwise the same experimental conditions. $L_W(HOM)$ represents wall loss rates that were measured from the decay of signal intensities after switching off HOM production. Since we know $L_W(HOM)$, $L_P(HOM)$ can be calculated by solving Equation S9 $L_P(HOM)$. Once knowing $L_W(HOM)$ and $L_P(HOM)$ as a function of particle surface allows extrapolating $c(HOM)^0$ from $c(HOM)$ measured during in any other experiment by using the ratio $c(HOM)^0/c(HOM)$ as correction factor. The values for

c*(HOM)*^{0}/c*(HOM)* were determined using the third term of equation S9 which is just the ratio of the total loss rate over the loss rate on particles.

The dependence of HOM concentrations on the turnover k_{OH}×[OH]×[MT] was determined in experiments by varying [OH]. The k_{OH} are the rate coefficients for the reaction of the respective MT with the OH radical (k_{OH} = 5.37×10^{-11} cm^3 s^{-1} (α-pinene) and 7.89×10^{-11} cm^3 s^{-1} (β-pinene), Atkinson, 1997). We varied [OH] by changing J(O^{1}D) at constant inflow of α-pinene or β-pinene. A non-linear dependence was found between c*(HOM)* and k_{OH}×[OH]×[α-/ β-pinene]. One reason for this non-linearity is HOM formation from ozonolysis reaction. We focus here on the method used to normalize the measured c*(HOM)* to a certain oxidation rate that was used as reference.

In double logarithmic plots of ln(c*(HOM)*) versus ln(k_{OH}×[OH]×[α-/ β-pinene]), we obtained linear relationships at high OH concentrations (> 10^7 cm^{-3}) when MT ozonolysis played only a minor role(<10%). For α-pinene we observed a strong contribution to HOM formation that was attributed to ozonolysis as shown in Figure S6 while for β-pinene the ozonolysis contribution was smaller.

The following analysis will be restricted to data where the turnover by OH was > 4.0×10^7 cm^{-3}s^{-1} and at least an order of magnitude higher than the oxidation rate by ozonolysis. This was the case for all our measurements with NO_X. Therefore we used the linear part of the curve shown in Figure S6 for normalization of α-pinene data.

Normalization was performed using Equation S10. To normalize the HOM signal intensities to turnover, we applied the slope (slp) of 1.47±0.07 of the power law plot (Figure S6):

$$c_R(HOM) = \frac{Tnv_R^{slp}}{Tnv_M^{slp}} \cdot c_M(HOM) \qquad \text{(S10)}$$

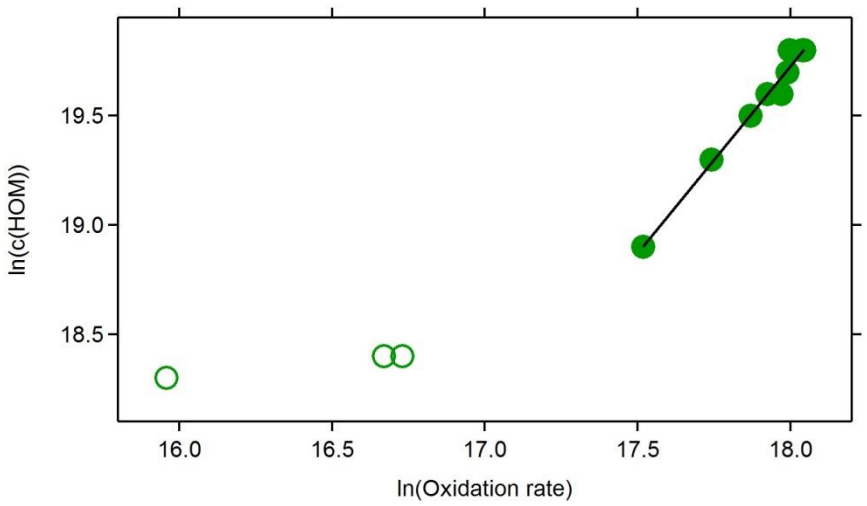

Figure S6: Plot of ln($c(HOM)$) versus ln(k_{OH}×[OH] ×[α-pinene]). Data were obtained from an experiment where [OH] was varied between 8.9×10^5 cm^{-3} and 4.8×10^7 cm^{-3} by varying J(O^{1}D). At OH oxidation rate <4.1×10^7 cm^{-3}s^{-1} which occurred at $[OH]_{SS}$ ~7.6×10^6 cm^{-3} and $[\alpha\text{-pinene}]_{SS}$ ~ 4.0 ppb HOM formation from ozonolysis interfered substantially with HOM formation from OH reactions and deviation from linearity appeared. ($[O_3]_{SS}$ varied from 14.6 to 25 ppb, caused by the variation of J(O^{1}D). Neglecting the data points at OH oxidation rate below 4.1×10^7 cm^{-3}s^{-1} (open circles), linear power law behavior was observed with a slope, slp = 1.47 ± 0.07.

In Equation S10, c_R(HOM) is the HOM concentration normalized to the turnover at the reference case with $Tnv_R \cdot c_M$(HOM) is the HOM mixing ratio measured during an experiment where the turnover is Tnv_R. As correction factor we used the ratio Tnv_R^{slp}/Tnv_M^{slp}. As the reference turnover, we used the largest turnover of 9.06×10^7 cm^{-3} s^{-1} at low NO_X conditions ([NO_X] ~ 0.3 ppb). The variation of Tnv_R^{slp}/Tnv_M^{slp} was less than 30% for the α-pinene systems. For the β-pinene systems we applied the same approach. The reference turnover Tnv_R was set to 2.19×10^8 cm^{-3} s^{-1} and the resulting slp = 3.8±0.5. The correction using the ratio Tnv_R^{slp}/Tnv_M^{slp} was less than 20% for the β-pinene systems.

Whenever it was necessary to normalize HOM mixing ratio to both, particle free conditions and to a certain turnover, we used the product of both correction factors. The HOM mixing ratio normalized to both, turnover and negligible particle surface, c(HOM) was calculated according to Equation S11 where c_M(HOM) is the measured mixing ratio.

$$c(HOM) = c_M(HOM) \cdot \frac{L_W(HOM)+L_P(HOM)}{L_P(HOM)} \cdot \frac{Tnv_R^{slp}}{Tnv_M^{slp}} \qquad \text{(S11)}$$

S4: Determination of HOM-ON and OrgNO_3 produced from β-pinene oxidation

The experiment described in Section 3.2 of the manuscript was performed by adding 39 ppb β-pinene ($[\beta\text{-pinene}]_0$), 50 ppb NO_X ($[NO_X]_0$) and 3.7 ppb m-xylene ($[\text{m-xylene}]_0$) to the chamber. In presence of OH these mixing ratios decreased to 6.5 ppb β-pinene, 20 ppb NO_X and 0.6 ppb m-xylene during steady state conditions. When the β-pinene inflow was removed from the chamber and the OH concentrations were adjusted to same values as before the removal, $[NO_X]$ was about 32 ppb.

At first we consider the system in absence of β-pinene (Figure 1, t ~ 3 h). In absence of β-pinene the loss of NO_X was determined by reactions of NO_2 with OH (R1), by reactions of NO_X with the peroxy radicals produced by photo-oxidation of m-xylene and by reactions of NO_2 with O_3.

Compared to the first two reactions, the reaction of NO_2 with O_3 is of minor importance for the NO_X balance. The oxidation rate of NO_2 by O_3 is about 4 times smaller than that by OH (R1) ($k_{O3+NO2} = 2.6\times10^{-17}$ cm^3 s^{-1}, IUPAC (2008); $[O_3] = 1.4\times10^{-12}$ ~ 60 ppb, oxidation rate 2.7×10^{7} cm^{-3} s^{-1}). Moreover, the NO_3 radicals formed in this reaction mostly either were photolyzed or reacted with NO, thus recycled to NO_X. We therefore neglected the reaction NO_2 with O_3.

Organic nitrates can be formed in reaction R5 and R6:

$$RO_2^{\cdot} + NO \rightarrow RONO_2 \qquad \text{(R5)}$$

$$RO_2^{\cdot} + NO_2 \leftrightarrow RO_2NO_2 \qquad \text{(R6)}$$

To keep the following rate equations simple we merged reactions R5 and R6 and describe the loss rates of NO_X due to both these reactions by $L(RO_2^c)$ where the index c stands for the respective compound (mx = m-xylene and b = β–pinene). The rate equation for NO_X in absence of β-pinene reads:

$$\frac{d[NO_X]}{dt} = \frac{F}{V} \cdot ([NO_X]_{in} - [NO_X]) - k_{NO2+OH} \cdot [OH] \cdot [NO_2] \; - L(RO_2^{mx}) \qquad \text{(S12)}$$

In Eq. S12, V is the volume of the chamber, F is the total air flow through the chamber, $[NO_X]$ is the concentration of NO_X in the chamber (measured at the chamber outlet) and $[NO_X]_{in}$ is the NO_X concentration at chamber inlet. The first term on the right side of equation S12 describes in- and outflow of NO_X, the second term describes the loss rate according to reaction R1 and the third term describes the loss rates of NO_X in reactions with peroxy radicals formed from m-xylene.

For steady state conditions we obtain:

$$\frac{F}{V} \cdot ([NO_X]_{in} - [NO_X]) = k_{NO2+OH} \cdot [OH] \cdot [NO_2] + L(RO_2^{mx}) \qquad \text{(S13)}$$

Data for the term on the left side of equation S13 were measured. For the rate coefficient of reaction R1 several values can be found in the literature. For example, applying a small rate coefficient ($k_{OH+NO2} = 6.8\times10^{-11}$ cm^3 s^{-1}, Burrows et al. (1983), NO_2 is oxidized at a rate of 1.04×10^8 cm^{-3} s^{-1}. Applying a high rate constant ($k_{OH+NO2} = 8.5\times10^{-11}$ cm^3 s^{-1}, Donahue et al. (1997), both rate coefficients for the 3rd order reaction include $M = 2.5\times10^{19}$ cm^{-3}) results in an oxidation rate of 1.3×10^8 cm^{-3} s^{-1}. Accordingly, reaction R1 could have caused a decrease of $[NO_X]$ between 12 and 15 ppb within the residence time of the air in the chamber.

During this phase of the experiment we measured a loss of NO_X of 18 ppb (see Figure 1 in the main text) and we attribute the remaining loss of 3 – 6 ppb to reactions of NO_X with peroxy radicals formed during photooxidation of m-xylene. Due to the uncertainty in the rate constants given for reaction R1, nothing can be concluded with respect to the yield of organic nitrate formation for m-xylene. However, we used the measured difference of 18 ppb for $[NOx]_{in} - [NO_X]$ as reference to calculate the yield of organic nitrate formation from β-pinene.

Because [OH] was re-adjusted after the removal of β-pinene, the respective m-xylene concentrations as well as its turnover was same as in the presence of β-pinene. Using the NO_X losses measured in the β-pinene free system therefore accounts for ON formation by m-xylene peroxy radicals. With β-pinene in the system the rate equation for NO_X reads:

$$\frac{d[NO_X]}{dt} = \frac{F}{V} \cdot ([NO_X]_{in} - [NO_X]) - k_{NO2+OH} \cdot [OH] \cdot [NO_2] - L(RO_2^{mx}) - L(RO_2^{b}) \qquad \text{(S14)}$$

$L(RO_2^{b})$ describes the loss rate of NO_X due to the formation of organic nitrates with peroxy radicals originating from β-pinene. For steady state it follows:

$$\frac{F}{V} \cdot ([NO_X]_{in} - [NO_X]) = k_{NO2+OH} \cdot [OH] \cdot [NO_2] + L(RO_2^{mx}) + L(RO_2^{b}) \quad \text{(S15)}$$

Organic nitrate formation from β-pinene was calculated from the difference $[NO_X]_{in} - [NO_X]$ at steady state conditions in presence and in absence of β-pinene, respectively. In presence of β-pinene the consumption of NO_X was higher by 12 ppb (Figure 1 of the main text).

For the experiment described in the main text we obtained a formation rate of: 1.07×10^8 cm^{-3} s^{-1}, i.e. about 12 ppb organic nitrates were formed within the residence time of the air in the chamber. Presuming that one NO_X molecule forms one organic nitrate molecule, the loss of 12 ppb NO_X is equivalent to the formation of 12 ppb of nitrate bound to organic moieties. With the nitrate molecular mass of 62 Da the total amount of nitrate bound to organic moieties ($OrgNO_3$) was around 33 µg m^{-3}.

By setting the formation of 12 ppb organic nitrates in relation to the consumption of 33 ppb β-pinene, we estimate the molecular yield of organic nitrate formation at the conditions of our experiment to about 36 %. For the steady state conditions with 20 ppb β-pinene we estimated the HNO_3 production. We used the average of the two rate constants given above for reaction R1 (k_{OH+NOX}=1.2E-11 cm^3 s^{-1}) and obtained $k_{OH+NOX}\times[OH]\times[NO_X]$ = 1.17×10^8 cm^{-3} s^{-1} which is equivalent to a production of ~ 9 ppb HNO_3 or ~24 µg m^{-3} within the residence time of the air in the chamber.

S5: Pattern of HOM-organic nitrates and determination of the median for their mass

Most of the literature data give the fractions of organic nitrates in SOA and not the fraction of organic bound nitrate ($OrgNO_3$). For better comparison of our data to literature data, we derived a factor to allow for conversion of the fraction of HOM-organic nitrates from the fraction of organic bound nitrate ($OrgNO_3$) and vice versa. This conversion factor is based on the mass of $OrgNO_3$ on the one hand and on the median mass of HOM-ON on the other hand. We take only HOM-ON with more than 6 O-atoms into account for determining their median mass since those HOM-ON would participate in particle mass formation. The conversion factor is determined for high NO_X levels when the pattern of organic nitrates is quite constant.

Figure S7 shows an extract of a mass spectrum from α-pinene photo-oxidation in presence of NO_X.

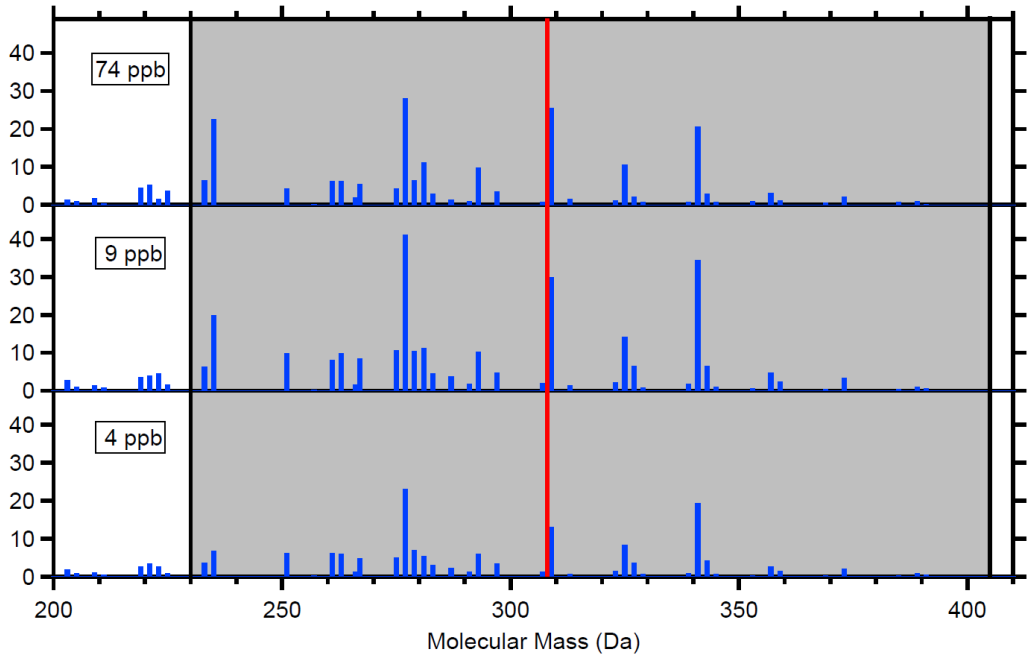

Figure S7: HOM-ON signal from α-pinene in the mass range between 200 Da and 405 Da. The stick height represents the integral of the fitted peak at high resolution. $[\alpha\text{-pinene}]_{SS}$ = 1.3 ppb, $[NO_X]_{SS}$ = 3.8-74 ppb. Dominant peaks are HOM-ON with the molecular formulas $C_{10}H_{15}O_XONO_2$ (X = 5, 7, and 9, masses 277, 309, and 341 Da).

In a first step the concentrations of HOM-ON were multiplied by their respective molecular mass to yield the mass concentrations. The mass concentrations were then normalized to total mass in the mass range from 230 to 405 Da.

$$c(HOM\text{-}ON)_i^{rel} \cdot m(HOM\text{-}ON)_i = \frac{c(HOM\text{-}ON)_i \cdot m(HOM\text{-}ON)_i}{\sum_i c(HOM\text{-}ON)_i \cdot m(HOM\text{-}ON)_i} \quad \text{(S16)}$$

The median was determined in the usual way, however, summing up to m = 307 Da led to ~ 39 %; summing up to m = 309 Da led to 53%. Reason for the large difference was the high abundance of the HOM-ON with the mass 309 Da ($C_{10}H_{15}O_7ONO_2$) (see Fig. S7). As the best value for a median mass of HOM-organic nitrates we choose 309 Da. This molecular mass still includes the mass of the nitrate (62 Da), therefore $OrgNO_3$ constitutes about 1/5 of the molecular mass of the median HOM-organic nitrate. To convert from mass fractions of $OrgNO_3$ (as measured by AMS) to mass fractions of HOM-ON we therefore multiply by 5, vice versa we divide by 5 (Section 4.1 of the main manuscript).

S6: Peak lists for α-pinene and β-pinene

Table S1 gives a peak list with assignments of molecular formulas to the integer masses of the respective HOM. The appearance of HOM monomers with less than 10 C-atoms indicates that these HOM went through a fragmentation process. We attribute their formation to alkoxy radical decomposition whereby the alkoxy radicals itself are produced in reaction R4 and R5. As decomposition of HOM alkoxy radicals also forms HOM-peroxy radicals with less than 10 C-atoms, also dimers with less than 20 C-atoms were found.

Table S1. 50 major peaks from peak list of α-pinene and β-pinene with and without NO_X addition *: no peak with clear identification and error below 15 ppm.

α-Pinene + OH							α-Pinene + OH + NOx						
	Formula	C	H	O	Detected mass(m/z)	HOM(Da)		Formula	C	H	O	N	Detected mass(m/z)	HOM(Da)
C_8	$C_8H_{10}O_8$	8	10	8	297.022	234.037	C_7	$C_7H_7NO_8$	7	7	8	1	296.003	233.017
	$C_8H_{10}O_9$	8	10	9	313.018	250.032		$C_7H_9NO_8$	7	9	8	1	298.018	235.033
	$C_8H_{12}O_8$	8	12	8	299.038	236.053		$C_7H_9NO_{10}$	7	9	10	1	330.008	267.023
	$C_8H_{12}O_9$	8	12	9	315.034	252.048	C_8	$C_8H_{10}O_8$	8	10	8	0	297.023	234.038
	$C_8H_{14}O_8$	8	14	8	301.054	238.068		$C_8H_{10}O_9$	8	10	9	0	313.018	250.032
C_9	$C_9H_{12}O_7$	9	12	7	295.043	232.058		$C_8H_{10}O_{12}$	8	10	12	0	361.003	298.017
	$C_9H_{12}O_8$	9	12	8	311.039	248.053		$C_8H_{11}O_{12}$	8	11	12	0	362.010	299.025
	$C_9H_{13}O_7$	9	13	7	296.051	233.066		$C_8H_{12}O_8$	8	12	8	0	299.039	236.053
	$C_9H_{13}O_8$	9	13	8	312.046	249.060		$C_8H_{13}NO_8$	8	13	8	1	314.050	251.064
	$C_9H_{13}O_9$	9	13	9	328.041	265.055	C_9	$C_9H_{11}O_{11}$	9	11	11	0	358.016	295.030
	$C_9H_{14}O_7$	9	14	7	297.059	234.073		$C_9H_{12}O_8$	9	12	8	0	311.039	248.053
	$C_9H_{14}O_8$	9	14	8	313.054	250.068		$C_9H_{12}O_{10}$	9	12	10	0	343.028	280.043
	$C_9H_{14}O_9$	9	14	9	329.049	266.063		$C_9H_{13}NO_8$	9	13	8	1	326.050	263.064
	$C_9H_{16}O_7$	9	16	7	299.074	236.089		$C_9H_{13}NO_9$	9	13	9	1	342.044	279.059
	$C_9H_{16}O_8$	9	16	8	315.070	252.085		$C_9H_{14}O_7$	9	14	7	0	297.059	234.074
C_{10}	$C_{10}H_{14}O_6$	10	14	6	293.064	230.078		$C_9H_{14}O_8$	9	14	8	0	313.054	250.069
	$C_{10}H_{14}O_7$	10	14	7	309.059	246.073		$C_9H_{14}O_9$	9	14	9	0	329.049	266.064
	$C_{10}H_{14}O_8$	10	14	8	325.054	262.069		$C_9H_{15}NO_9$	9	15	9	1	344.060	281.075
	$C_{10}H_{14}O_9$	10	14	9	341.049	278.063		$C_9H_{15}NO_{10}$	9	15	10	1	360.055	297.070
	$C_{10}H_{14}O_{10}$	10	14	10	357.044	294.058	C_{10}	$C_{10}H_{13}NO_8$	10	13	8	1	338.050	275.064
	$C_{10}H_{15}O_7$	10	15	7	310.067	247.081		$C_{10}H_{14}O_7$	10	14	7	0	309.059	246.074
	$C_{10}H_{15}O_9$	10	15	9	342.056	279.071		$C_{10}H_{14}O_8$	10	14	8	0	325.054	262.069
	$C_{10}H_{15}O_{10}$	10	15	10	358.051	295.066		$C_{10}H_{14}O_9$	10	14	9	0	341.049	278.064
	$C_{10}H_{16}O_6$	10	16	6	295.080	232.094		$C_{10}H_{14}O_{10}$	10	14	10	0	357.044	294.059
	$C_{10}H_{16}O_7$	10	16	7	311.074	248.089		$C_{10}H_{14}O_{11}$	10	14	11	0	373.039	310.054
	$C_{10}H_{16}O_8$	10	16	8	327.070	264.085		$C_{10}H_{15}NO_7$	10	15	7	1	324.070	261.085
	$C_{10}H_{16}O_9$	10	16	9	343.064	280.079		$C_{10}H_{15}NO_8$	10	15	8	1	340.065	277.080
	$C_{10}H_{16}O_{10}$	10	16	10	359.059	296.074		$C_{10}H_{15}NO_9$	10	15	9	1	356.060	293.075
	$C_{10}H_{16}O_{11}$	10	16	11	375.054	312.069		$C_{10}H_{15}NO_{10}$	10	15	10	1	372.055	309.070
	$C_{10}H_{17}O_{10}$	10	17	10	360.067	297.082		$C_{10}H_{15}NO_{11}$	10	15	11	1	388.050	325.065
	$C_{10}H_{18}O_6$	10	18	6	297.095	234.110		$C_{10}H_{15}NO_{12}$	10	15	12	1	404.045	341.059
	$C_{10}H_{18}O_7$	10	18	7	313.090	250.105		$C_{10}H_{15}NO_{13}$	10	15	13	1	420.040	357.054
	$C_{10}H_{18}O_8$	10	18	8	329.085	266.100		$C_{10}H_{15}O_7$	10	15	7	0	310.067	247.082
	$C_{10}H_{18}O_{10}$	10	18	10	361.075	298.089		$C_{10}H_{15}O_{10}$	10	15	10	0	358.052	295.067
C_{16}	$C_{16}H_{24}O_{12}$	16	24	12	471.112	408.126		$C_{10}H_{15}O_{11}$	10	15	11	0	374.047	311.061
C_{17}	$C_{17}H_{24}O_{12}$	17	24	12	483.112	420.126		$C_{10}H_{16}O_7$	10	16	7	0	311.075	248.090
	$C_{17}H_{26}O_{10}$	17	26	10	453.137	390.152		$C_{10}H_{16}O_8$	10	16	8	0	327.070	264.085
	$C_{17}H_{26}O_{11}$	17	26	11	469.132	406.147		$C_{10}H_{16}O_9$	10	16	9	0	343.065	280.079
C_{18}	$C_{18}H_{28}O_{12}$	18	28	12	499.143	436.158		$C_{10}H_{16}O_{10}$	10	16	10	0	359.060	296.074
C_{19}	$C_{19}H_{28}O_{11}$	19	28	11	495.148	432.163		$C_{10}H_{16}O_{11}$	10	16	11	0	375.055	312.069
	$C_{19}H_{28}O_{12}$	19	28	12	511.143	448.158		$C_{10}H_{17}O_8$	10	17	8	0	328.078	265.092
	$C_{19}H_{28}O_{13}$	19	28	13	527.138	464.152		$C_{10}H_{17}NO_7$	10	17	7	1	326.086	263.101
	$C_{19}H_{30}O_{12}$	19	30	12	513.159	450.173		$C_{10}H_{17}NO_8$	10	17	8	1	342.081	279.095
	$C_{19}H_{30}O_{13}$	19	30	13	529.154	466.168		$C_{10}H_{17}NO_{11}$	10	17	11	1	390.066	327.080
C_{20}	$C_{20}H_{30}O_9$	20	30	9	477.174	414.188		$C_{10}H_{17}NO_{12}$	10	17	12	1	406.060	343.075
	$C_{20}H_{30}O_{11}$	20	30	11	509.164	446.178	C_{11}	$C_{11}H_{14}O_{13}$	11	14	13	0	417.029	354.043
	$C_{20}H_{30}O_{13}$	20	30	13	541.154	478.168		$C_{11}H_{16}O_8$	11	16	8	0	339.070	276.085
	$C_{20}H_{32}O_9$	20	32	9	479.189	416.204		$C_{11}H_{16}O_9$	11	16	9	0	355.065	292.079
	$C_{20}H_{32}O_{11}$	20	32	11	511.179	448.194		$C_{11}H_{16}O_{10}$	11	16	10	0	371.060	308.074
	$C_{20}H_{32}O_{12}$	20	32	12	527.174	464.189		$C_{11}H_{16}O_{13}$	11	16	13	0	419.044	356.059

* These compounds have less certainty.

β-Pinene + OH								β-Pinene + OH + NOx							
	Formula	C	H	O	N	Detected mass(m/z)	HOM(Da)		Formula	C	H	O	N	Detected mass(m/z)	HOM(Da)
C_7	$C_7H_9O_{11}$	7	9	11	0	331.003	269.014	C_6	$C_6H_7NO_{10}$	6	7	10	1	314.995	253.007
	$C_7H_{10}O_9$	7	10	9	0	300.021	238.032		$C_6H_7NO_{11}$	6	7	11	1	330.990	269.002
	$C_7H_{11}O_9$	7	11	9	0	301.029	239.040	C_7	$C_7H_9NO_8$	7	9	8	1	297.021	235.033
C_8	$C_8H_{10}O_8$	8	10	8	0	296.026	234.038		$C_7H_9NO_{10}$	7	9	10	1	329.011	267.023
	$C_8H_{11}O_8$	8	11	8	0	297.034	235.045		$C_7H_{10}NO_{12}$*	7	10	12	1	362.009	300.020
	$C_8H_{11}O_9$	8	11	9	0	313.029	251.040		$C_7H_{11}NO_8$	7	11	8	1	299.037	237.048
	$C_8H_{12}O_9$	8	12	9	0	314.037	252.048		$C_7H_{11}NO_9$	7	11	9	1	315.032	253.043
	$C_8H_{12}O_{10}$	8	12	10	0	330.031	268.043		$C_7H_{11}NO_{10}$	7	11	10	1	331.027	269.038
	$C_8H_{13}O_9$	8	13	9	0	315.044	253.056	C_8	$C_8H_{10}O_8$	8	10	8	0	296.026	234.038
C_9	$C_9H_{11}O_{11}$	9	11	11	0	357.018	295.030		$C_8H_{10}O_{11}$	8	10	11	0	344.011	282.022
	$C_9H_{12}O_7$	9	12	7	0	294.047	232.058		$C_8H_{12}O_9$	8	12	9	0	314.037	252.048
	$C_9H_{12}O_8$	9	12	8	0	310.042	248.053		$C_8H_{12}O_{10}$	8	12	10	0	330.031	268.043
	$C_9H_{12}O_9$	9	12	9	0	326.037	264.048	C_9	$C_9H_{12}O_9$	9	12	9	0	326.037	264.048
	$C_9H_{12}O_{10}$	9	12	10	0	342.031	280.043		$C_9H_{12}O_{10}$	9	12	10	0	342.031	280.043
	$C_9H_{12}O_{11}$	9	12	11	0	358.026	296.038		$C_9H_{13}NO_9$	9	13	9	1	341.047	279.059
	$C_9H_{13}O_8$	9	13	8	0	311.049	249.061		$C_9H_{13}NO_{10}$	9	13	10	1	357.042	295.054
	$C_9H_{13}O_9$	9	13	9	0	327.044	265.056		$C_9H_{13}NO_{11}$	9	13	11	1	373.037	311.049
	$C_9H_{14}O_7$	9	14	7	0	296.062	234.074		$C_9H_{13}NO_{12}$	9	13	12	1	389.032	327.044
	$C_9H_{14}O_8$	9	14	8	0	312.057	250.069		$C_9H_{14}O_9$	9	14	9	0	328.052	266.064
	$C_9H_{14}O_9$	9	14	9	0	328.052	266.064		$C_9H_{14}O_{10}$	9	14	10	0	344.047	282.059
	$C_9H_{14}O_{10}$	9	14	10	0	344.047	282.059		$C_9H_{15}NO_9$	9	15	9	1	343.063	281.075
	$C_9H_{15}O_7$	9	15	7	0	297.070	235.082		$C_9H_{15}NO_{10}$	9	15	10	1	359.058	297.070
	$C_9H_{15}O_{12}$	9	15	12	0	377.045	315.056		$C_9H_{15}NO_{11}$	9	15	11	1	375.053	313.065
	$C_9H_{16}O_8$	9	16	8	0	314.073	252.085	C_{10}	$C_{10}H_{14}O_8$	10	14	8	0	324.057	262.069
	$C_9H_{16}O_9$	9	16	9	0	330.068	268.079		$C_{10}H_{14}O_9$	10	14	9	0	340.052	278.064
C_{10}	$C_{10}H_{14}O_7$	10	14	7	0	308.062	246.074		$C_{10}H_{14}O_{10}$	10	14	10	0	356.047	294.059
	$C_{10}H_{14}O_8$	10	14	8	0	324.057	262.069		$C_{10}H_{14}O_{11}$	10	14	11	0	372.042	310.054
	$C_{10}H_{14}O_9$	10	14	9	0	340.052	278.064		$C_{10}H_{14}O_{12}$	10	14	12	0	388.037	326.049
	$C_{10}H_{14}O_{10}$	10	14	10	0	356.047	294.059		$C_{10}H_{14}O_{13}$	10	14	13	0	404.032	342.043
	$C_{10}H_{14}O_{11}$	10	14	11	0	372.042	310.054		$C_{10}H_{14}O_{14}$	10	14	14	0	420.027	358.038
	$C_{10}H_{15}O_8$	10	15	8	0	325.065	263.077		$C_{10}H_{15}NO_9$	10	15	9	1	355.063	293.075
	$C_{10}H_{15}O_9$	10	15	9	0	341.060	279.072		$C_{10}H_{15}NO_{10}$	10	15	10	1	371.058	309.070
	$C_{10}H_{15}O_{10}$	10	15	10	0	357.055	295.067		$C_{10}H_{15}NO_{11}$	10	15	11	1	387.053	325.065
	$C_{10}H_{15}O_{11}$	10	15	11	0	373.050	311.061		$C_{10}H_{15}NO_{12}$	10	15	12	1	403.048	341.059
	$C_{10}H_{15}O_{12}$	10	15	12	0	389.045	327.056		$C_{10}H_{15}NO_{13}$	10	15	13	1	419.043	357.054
	$C_{10}H_{15}NO_{10}$	10	15	10	1	371.058	309.070		$C_{10}H_{16}O_8$	10	16	8	0	326.073	264.085
	$C_{10}H_{15}NO_{11}$	10	15	11	1	387.053	325.065		$C_{10}H_{16}O_9$	10	16	9	0	342.068	280.079
	$C_{10}H_{16}O_7$	10	16	7	0	310.078	248.090		$C_{10}H_{16}O_{10}$	10	16	10	0	358.063	296.074
	$C_{10}H_{16}O_8$	10	16	8	0	326.073	264.085		$C_{10}H_{16}O_{11}$	10	16	11	0	374.058	312.069
	$C_{10}H_{16}O_9$	10	16	9	0	342.068	280.079		$C_{10}H_{17}NO_9$	10	17	9	1	357.079	295.090
	$C_{10}H_{16}O_{10}$	10	16	10	0	358.063	296.074		$C_{10}H_{17}NO_{10}$	10	17	10	1	373.074	311.085
	$C_{10}H_{17}O_9$	10	17	9	0	343.076	281.087	C_{11}	$C_{11}H_{14}O_{12}$	11	14	12	0	400.037	338.049
C_{17}	$C_{17}H_{26}O_{12}$	17	26	12	0	484.131	422.142		$C_{11}H_{15}O_{16}$	11	15	16	0	465.024	403.036
C_{18}	$C_{18}H_{26}O_9$	18	26	9	0	448.146	386.158		$C_{11}H_{16}O_{10}$	11	16	10	0	370.063	308.074
	$C_{18}H_{26}O_{10}$	18	26	10	0	464.141	402.153		$C_{11}H_{16}O_{11}$	11	16	11	0	386.058	324.069
	$C_{18}H_{26}O_{11}$	18	26	11	0	480.136	418.147		$C_{11}H_{16}O_{12}$*	11	16	12	0	402.053	340.064
	$C_{18}H_{26}O_{12}$	81	26	12	0	496.131	434.142		$C_{11}H_{16}O_{13}$	11	16	13	0	418.047	356.059
C_{19}	$C_{19}H_{28}O_{10}$	19	28	10	0	478.157	416.168		$C_{11}H_{16}O_{14}$	11	16	14	0	434.042	372.054
	$C_{19}H_{28}O_{11}$	19	28	11	0	494.152	432.163		$C_{11}H_{18}O_{13}$	11	18	13	0	420.063	358.075
	$C_{19}H_{30}O_{12}$	19	30	12	0	512.162	450.174	C_{12}	$C_{12}H_{19}O_{15}$*	12	19	15	0	465.061	403.072

* These compounds have less certainty.

References in supplement (if not referenced in the manuscript):

Atkinson, R., Baulch, D. L., Cox, R. A., Crowley, J. N., Hampson, R. F., Hynes, R. G., Jenkin, M. E., Rossi, M. J., and Troe, J.: Evaluated kinetic and photochemical data for atmospheric chemistry: Volume I - gas phase reactions of O-x, HOx, NOx and SOx species, Atmos. Chem. Phys., 4, 1461-1738, doi: 10.5194/acp-4-1461-2004, 2004.

Burrows, J. P., Wallington, T. J., and Wayne, R. P.: J. Chem. Soc. Faraday Trans. , 2, 79, 111-122, doi: 10.1039/f29837900111, 1983.

Donahue, N. M., Dubey, M. K., Mohrschladt, R., Demerjian, K., and Anderson, J. G.: J. Geophys. Res., 102, 6159-6168, doi: 10.1029/96JD02329, 1997.

IUPAC Subcommittee on Gas Kinetic Data Evaluation, 2008.

Long, B., Bao, J. L., and Truhlar, D. G.: Reaction of SO_2 with OH in the atmosphere. Phys Chem. Chem. Phys., 19, 8091-8100, doi: 10.1039/c7cp00497d, 2017.

MCM Version 3.2, http://mcm.leeds.ac.uk/MCMv3.2/ .

Stark, H., Yatayelli, R. L. N., Thompson, S. L., Kimmel, J. R., Cubison, M. J., Chhabra, P. S., Canagaratna, M. R., Jayne, J. T., Worsnop, D. R., and Jimenez, J. L.: Methods to extract molecular and bulk chemical information from series of complex mass spectra with limited mass resolution, Int. J. Mass Spectrom., 389, 26–38, doi:10.1016/j.ijms.2015.08.011, 2015.